Imperial College London

Master's Thesis

Confinement and the String Tension in Hot Yang Mills

Author:
Cian O Hara

Supervisor:
Dr. Arttu Rajantie

Submitted in partial fulfilment of the requirements
for the degree of Master of Science of Imperial College London

September 2013

Contents

1 Introduction **1**

2 Lattice Field Theory **3**
2.1 Scalar Fields . . . 3
2.2 Gauge Fields . . . 7

3 Wilson Loops and Polyakov lines **13**
3.1 Wilson Loops . . . 13
3.2 Polyakov Loops . . . 16
3.3 Centre Symmetry . . . 18
3.4 Magnetic Monopoles and Centre Vortices . . . 19

4 Monte Carlo Simulations **21**
4.1 Importance Sampling and the Monte Carlo Method . . . 21
4.2 Markov Chains . . . 22
4.3 The Metropolis Algorithm . . . 23
4.4 The Heat Bath Algorithm . . . 25
4.5 Error analysis and autocorrelation . . . 26
4.6 Summary . . . 27

5 Results **29**
5.1 String tension at zero temperature . . . 29
5.2 Phase transition at non-zero temperature . . . 31

6 Discussion and Further Analysis. **35**

Bibliography **37**

Chapter 1

Introduction

The Standard Model of particle physics is currently our best description of how sub-atomic particles, such as quarks, interact. It describes three out of the four fundamental forces of nature, electromagnetism and the strong and weak nuclear forces, to extremely high accuracy over a large range of energies.

The strong force deals with quarks and gluons and is responsible for holding together the constituents of the atoms which make up all of the matter we see around us. Based on an SU(3) colour gauge theory, the strong force exhibits what is known as confinement and asymptotic freedom. This is related to the fact that the the SU(3) gauge group is non-abelian, leading to gluon-gluon interactions. At large distances quark interactions become strong and perturbative expansions become useless in describing the physics of the system. This leads to the idea that isolated quarks cannot exist in nature, known as confinement. The absence of any isolated quarks seen in experiments supports this idea. At short distances and high energies, where a perturbative expansion is valid, the quarks become asymptotically free and we see the phenomenon of deconfinement.

As in any field theory, naive analytical calculations lead to various ultraviolet and infrared divergences, which must be dealt with. For the theory to be defined in a mathematically rigorous way we must regularize it by introducing a regulator. There are many different schemes for regularization, for example dimensional regularization or Pauli-Villars regularization.

The scheme chosen in this dissertation, introduced by Wilson [1], is known as Lattice Regularization. This involves modelling spacetime, not as a continuum, but on a finite

lattice made up of discrete points at a finite distance from each other. We then discretize the theory on this lattice. This method is useful in that it lends itself to numerical analysis. It also preserves manifest gauge invariance and so there is no need for the standard gauge fixing procedure. It does, however, break Poincaré invariance, which is only recovered upon renormalizing our theory. Taking the limit where the spatial extent of the lattice goes to infinity and the lattice spacing between the points goes to zero effectively brings us back to the continuum.

In this analysis we will not focus on the SU(3) gauge group of QCD but instead focus on the simpler but still physically relevant SU(2) theory without dynamical quarks, or colour sources. We will briefly discuss the basic theory behind discretizing a gauge theory on a lattice and then move on to numerical results for observables computed as averages over configurations of the gauge field on the lattice.

The main observable we will be interested in is the Wilson loop. From this we will compute the string tension σ defined as the coefficient of the long range linear potential felt by separated quarks. The string tension is a useful order parameter in that it can easily be used to distinguish between confined and deconfined phases. We examine the effect that different lattice sizes and shapes have on the string tension effectively simulating our theory at a range of temperatures. We will see that for low energies, pure SU(2) gauge theory is indeed confining and that at a certain critical inverse coupling, β_c, the theory undergoes a phase transition from a confining to a deconfined phase signalled by the string tension going to zero.

Chapter 2

Lattice Field Theory

We want to measure physical observables, such as the Wilson Loop, computationally on a lattice. To do this, we will need to be able to relate our formulae for correlation functions from continuum quantum field theory to ones we can realise on the lattice. In this chapter, I will briefly explain how such a relation is formed. We find ultimately that a field theory discretized on a Euclidean lattice can be thought of as a quantum statistical mechanical system.

2.1 Scalar Fields

To start I will briefly review path integral quantization in the case of both a one dimensional quantum mechanical system and for a scalar field theory. A fuller treatment can be found in many texts, for example [2].

We consider first a single particle with Hamiltonian $\hat{H}(p, q)$ in one dimensional quantum mechanics. Evolution in time is described by the operator

$$\hat{U}(t) = \exp(-i\hat{H}t) \tag{2.1.1}$$

and the amplitude to propagate from q_1 to q_2 is given by

$$U(q_1, q_2; t) = \langle q_2|\hat{U}(t)|q_1\rangle. \tag{2.1.2}$$

By dividing the time interval into N segments of duration $\epsilon = t/N$, taking ϵ to be infinitesimally small, and integrating over all q(t) we get the familiar path integral expression for the amplitude,

$$U(q_1, q_2; t) = \int_{q_1}^{q_2} \mathcal{D}q(t)\ \exp(iS). \tag{2.1.3}$$

Here S is the theory's action and $\mathcal{D}q(t) = \prod_i dq_i(t)$. The amplitude is an integral over all possible paths $q_i(t)$ from q_1 to q_2 weighted by a highly oscillatory exponential function. To remedy this we make a Wick rotation where $t \to -it$. This gives us what is known as the Euclidean path integral and action, as the metric tensor is now given by $\delta_{\mu\nu}$. The path integral is then given with the Euclidean S_E action as

$$Z = \int_{q_1}^{q_2} \mathcal{D}q(t)\ \exp(-S_E). \tag{2.1.4}$$

This integral is real and bounded, making theoretical and computational work much easier. We will refer to this as the "partition function" for our theory. After moving to imaginary time, for $\epsilon = t/N$, 2.1.2 becomes

$$\langle q_2|U(\epsilon).....U(\epsilon)|q_1\rangle = \langle q_2|\exp(-\hat{H}\epsilon)^N|q_1\rangle, \tag{2.1.5}$$

where $\exp(-\hat{H}\epsilon) = \hat{T}$ is known as the transfer operator. It describes the evolution of our system in an infinitesimal time step ϵ. We know in quantum statistical mechanics that we can write the partition function for a system at temperature β_T^{-1} as

$$Z = \mathrm{tr}[\exp(-\beta H)], \tag{2.1.6}$$

and taking $\beta = t = N\epsilon$ we see

$$Z = \mathrm{tr}[\exp(-\hat{H}\epsilon)^N] = \int \mathrm{d}q\ \langle q|\exp(-\hat{H}\epsilon)^N|q\rangle. \tag{2.1.7}$$

This is just our path integral 2.1.4 with $q_1 = q_2 = q$ with periodic boundary conditions. This is the reason for calling 2.1.4 the partition function and motivates the idea of using concepts from statistical mechanics in analysing our theory on a lattice.

This process is straight forward to generalise to the case of a scalar field. $q(t)$ is replaced by $\phi(x)$ and the partition function becomes

$$Z = \int \mathcal{D}\phi \, \exp(-S_E). \tag{2.1.8}$$

The standard Euclidean action of ϕ^4 theory is given by

$$S_E(\phi(x)) = \int dx_4 \int d^3x \left(\frac{1}{2}\partial_\mu \phi(x) \partial^\mu \phi(x) - \frac{m^2}{2}\phi(x)^2 - \frac{\lambda}{4}\phi(x)^4 \right). \tag{2.1.9}$$

Again a rotation to imaginary time has been performed. For most purposes this is sufficient to extract any relevant physical information from the theory. However if necessary, one may rotate back to real time using the reverse rotation.

In the previous case we divided t into N segments of length ϵ, effectively discretizing the quantum mechanical system on a Euclidean time lattice. In analogy, we will now discretize each of the 4 spacetime dimensions. The scalar field is restricted to a finite set of points, x_μ, on a hypercubic lattice of side $L = na$ with spacetime volume L^4. The points are given by

$$x_\mu = a m_\mu \qquad \text{where} \qquad m_\mu = 0, 1, ..., n-1.$$

Here a is the spacing between neighboring lattice points. It is sometimes necessary to take different lattice spacings for the time and spatial directions, for example, to simulate the theory at a non-zero temperature. In this case one takes $N_t < N_s$, i.e. the number of points in the time direction is less than in the spatial directions. We will come back to this later.

On going to momentum space, we can see that a non-zero lattice spacing corresponds to a finite momentum cutoff on the order of a^{-1}. For example, for a one dimensional function defined only on a finite set of points $x = na$ the Fourier transform is given by

$$f(na) = \int_{-\pi/a}^{\pi/a} \frac{\mathrm{d}k}{2\pi} \tilde{f}_a(k) e^{ikna} \tag{2.1.10}$$

So we immediately see that momentum integrals are restricted to a finite domain, naturally regularizing any ultraviolet divergences. The continuum limit is recovered by taking $a \to 0$ and $L \to \infty$. This is obviously impossible to simulate on a computer. However for many studies the finiteness of the lattice is negligible.

To discretize the action on the lattice we replace derivatives by finite differences

$$\partial_\mu \phi(x) \longrightarrow \frac{1}{a}(\phi(x + \hat{\mu}) - \phi(x))$$

where $\hat{\mu}$ is a unit vector in the μ direction. The fields and constants are scaled so that the overall action remains dimensionless.

$$\tilde{\phi}(x) = \frac{\phi(x)}{a} \qquad \tilde{m} = \frac{m}{a}$$

Integrals are replaced by sums and the measure involves only lattice points x.

$$\int d^4x = a^4 \sum_x = a^4 \sum_{m_1=0}^{N-1} ... \sum_{m_4=0}^{N-1} \qquad \mathcal{D}\phi(x) = \prod_x d\phi(x)$$

Our discretized euclidean action is then given by

$$S_E = a^4 \sum_x \left(\frac{1}{2} \sum_{\mu=1}^{4} \left(\frac{\tilde{\phi}(x + \hat{\mu}) - \tilde{\phi}(x)}{a} \right)^2 + \frac{\tilde{m}^2}{2} \tilde{\phi}(x)^2 - \frac{\lambda}{4} \tilde{\phi}(x)^4. \right). \tag{2.1.11}$$

Correlation functions, derived in many text such as [2], for continuum QFT in real time are given as

$$\langle \phi(x_1)\phi(x_2)....\rangle = \frac{\int \mathcal{D}\phi \phi(x_1)\phi(x_2)....e^{iS(\phi)}}{\int \mathcal{D}\phi e^{iS}} \tag{2.1.12}$$

On the lattice, with discretized Euclidean action, the two point correlation function is written as

$$\frac{1}{Z}\int \prod_x d\phi(x)\phi(x_1)\phi(x_2)\ \exp(-S_E). \tag{2.1.13}$$

We again see the similarity with the expectation value of an observable from a statistical mechanical system computed on a configuration of "spins" on a Euclidean lattice,

$$\langle O\rangle = \frac{1}{Z}\mathrm{tr}[O(s)\ \exp(-\beta H(s))] \longleftrightarrow \frac{1}{Z}\int \prod_x d\phi(x) O(\phi)\ \exp(-S_E). \tag{2.1.14}$$

Due to these similarities we can use well known Monte Carlo methods from statistical mechanics to measure any observables which are functions of the fields on the lattice. We will call one set of field values on our lattice a configuration and the sum over all such configurations gives us the partition function for the system.

2.2 Gauge Fields

I will briefly recap continuum QCD and then show how it is realised on the lattice. The main difference is that we now have to include both the fermionic and gauge fields on the lattice. We will see that this is done by restricting the fermions to the lattice points as before. However for the gauge field we will instead associate it with the links between lattice points.

The following will be for SU(N) colour symmetry, the group of unitary N x N matrices with determinant 1. We will then specialise to the case of $N = 2$.

We introduce the quark field $\psi^{\alpha f c}(x)$. Here α is a Dirac index running from 1 to 4, f is the quark "flavour" index and c is the colour index. The SU(N) matrices act only on the colour index. I will suppress the indices from here on.

We insist that the action for the theory is invariant under local gauge transformations of the form

$$\psi(x) \longrightarrow \Lambda(x)\psi(x) \qquad \bar{\psi}(x) \longrightarrow \bar{\psi}(x)\Lambda^\dagger(x)$$

where Λ is a member of the gauge group. In the usual way, we introduce a gauge field G_μ and define the standard covariant derivative D_μ by

$$D_\mu = \partial_\mu - iG_\mu \tag{2.2.1}$$

.

For the action to be gauge invariant we find D_μ and G_μ must transform as

$$D_\mu \longrightarrow \Lambda(x) D_\mu \Lambda^\dagger(x) \qquad G_\mu \longrightarrow \Lambda(x) G_\mu \Lambda^\dagger(x) + i\Lambda(x)\partial_\mu \Lambda^\dagger(x) \tag{2.2.2}$$

G_μ is a lie algebra valued matrix gauge field, so it can be written as a sum over the generators for su(N). From the commutator $[D_\mu, D_\nu]$ we make a field tensor $G_{\mu\nu}$ which transforms in the same way as D_μ and allows us to write a gauge invariant term, tr $G_{\mu\nu}G^{\mu\nu}$. Using the fact that for the generators T_k of su(N) we have tr$[T_k, T_l] = \delta_{kl}$ we get the standard gauge invariant QCD Lagrangian,

$$S = \int d^4x \left(\frac{1}{4g^2} \sum_{k=1}^{8} G^k_{\mu\nu} G^{k\mu\nu} + \bar{\psi}\gamma^\mu D_\mu \psi + \bar{\psi} m \psi \right). \tag{2.2.3}$$

We discretize this, as before, by restricting $\psi(x)$ to the set of points on a hypercubic lattice of side $L = na$. However, now we have a problem. Terms of the form $\bar{\psi}(x)\psi(x+\hat{\mu})$, which arise in the kinetic term for the quarks, are no longer gauge invariant, as

$$\bar{\psi}(x)\psi(x+\hat{\mu}) \longrightarrow \bar{\psi}(x)\Lambda^\dagger(x)\Lambda(x+\hat{\mu})\psi(x+\hat{\mu}).$$

To counter this we introduce the gauge group valued field $U_\mu(x)$. The "link variable" $U_\mu(x)$ is assigned to the link between the lattice site x and $x+\hat{\mu}$. The link variable going in the opposite direction, ie. from $x+\hat{\mu}$ to x, is given by $U^\dagger_\mu(x) = U_{-\mu}(x+\hat{\mu})$ as shown in Figure: 2.1. We see that $\bar{\psi}(x)U_\mu(x)\psi(x+\hat{\mu})$ is now gauge invariant provided $U_\mu(x)$ transforms as

$$U_\mu(x) \longrightarrow \Lambda(x) U_\mu(x) \Lambda^\dagger(x+\hat{\mu}). \tag{2.2.4}$$

FIGURE 2.1: The link variables $U_\mu(x)$ and $U_\mu^\dagger(x)$

To make a connection between the link variables and the gauge field $G_\mu(x)$ in the continuum we introduce the concept of a gauge transporter. A gauge transporter from the point x to y, along the path C, is given by

$$U_C(x,y) = \mathrm{P}\ \exp\left(i\int_C dx_\mu G^\mu(x)\right), \tag{2.2.5}$$

where the P stands for path ordering of the exponential. It relates the points x and $x+\hat{\mu}$ similar to how parallel transport relates points on a manifold. It has the properties

1. $U_C(x,x) = 1$
2. $U_C(x,y)U_C(y,z) = U_C(x,z)$
3. $U_C(y,x) = U_C^{-1}(x,y)$

We note that, under a gauge transformation, $U_C(x,y)$ transforms as

$$U_C(x,y) \longrightarrow \Lambda(x)U_C(x,y)\Lambda^\dagger(y). \tag{2.2.6}$$

Comparing with 2.2.4, we see we can think of $U_\mu(x)$ as a lattice version of the gauge transporter from the point x to the point $x+\hat{\mu}$. This is the reason why it is associated with the link between the two points. To $\mathcal{O}(a)$ we can approximate the integral by the value of G_μ at the point x times the length of the path,

$$U_\mu(x) = \exp(iaG_\mu(x)). \tag{2.2.7}$$

A path between any two points on the lattice can be made by multiplication of individual link variables. Consider the L shaped path starting at x, moving one lattice spacing in the $\hat{\mu}$ direction and then one in the $\hat{\nu}$ direction. This will again transform in the correct way.

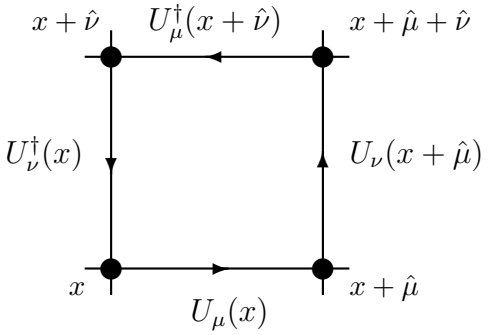

FIGURE 2.2: An elementary Plaquette $U_{\mu\nu}(x)$

$$U_\mu(x)U_\nu(x+\hat{\mu}) \longrightarrow \Lambda(x)U_\mu(x)\Lambda^\dagger(x+\hat{\mu})\Lambda(x+\hat{\mu})U_\nu(x+\hat{\mu})\Lambda^\dagger(x+\hat{\mu}+\hat{\nu}).$$

$$= \Lambda(x)U_\mu(x)U_\nu(x+\hat{\mu})\Lambda^\dagger(x+\hat{\mu}+\hat{\nu}) \tag{2.2.8}$$

The same is true for any path made up of individual links. All of the gauge rotations will cancel except at the end points. The order here is important as in general the elements do not commute.

Paths that start and end on the same point are of particular interest as they can be made into gauge invariant objects by taking a trace. The simplest such path, a square of side a, is known as a plaquette and is denoted by $U_{\mu\nu}(x)$. It is formed from the product of the four link variables around the square in the order they are encountered, shown in Figure: 2.2,

$$U_{\mu\nu}(x) = U_\mu(x)U_\nu(x+\hat{\mu})U_\mu^\dagger(x+\hat{\nu})U_\nu(x)^\dagger. \tag{2.2.9}$$

Using this we can write down a gauge invariant action known as Wilson's action. It is a sum over all the individual plaquettes on the lattice and is given as, for SU(N)

$$S(U) = \frac{\beta}{N}\sum_x \sum_{\mu<\nu} \text{Re tr}[1 - U_{\mu\nu}(x)]. \tag{2.2.10}$$

.

β here, not to be confused with the inverse temperature mentioned earlier, is known as the inverse coupling. Expanding 2.2.7 and using the Baker-Campbell-Hausdorff formula, we find

$$U_{\mu\nu}(x) = \exp(ia^2 G_{\mu\nu}(x) + O(a^3)). \tag{2.2.11}$$

$G_{\mu\nu}(x)$ here is the obvious discretized version of the continuum field strength tensor. If we take $\beta = 2N/g^2$ Wilson's action becomes

$$\frac{a^4}{2g^2} \sum_x \sum_{\mu<\nu} \mathrm{tr}[G_{\mu\nu}(x)^2] + O(a^2). \tag{2.2.12}$$

So we see that in the continuum limit 2.2.10 reduces to the Yang Mills part of 2.2.3

$$S_G = \frac{1}{4g^2} \sum_{k=1}^{8} \int d^4x \; G^k_{\mu\nu} G^{k\mu\nu}. \tag{2.2.13}$$

From here on we will use this action to focus on pure gauge theory, or gluondynamics, on the lattice. To do this we will assume that our quarks, or colour sources, are infinitely heavy and don't play any dynamical role in the physics of our system. A naive discretization, using the machinery discussed up until here, of the rest of 2.2.3 leads to extra problems, such as fermion doubling, which are beyond the scope of this analysis.

We may now use 2.1.14 to compute expectation values of observables which are functions of the gauge field

$$\langle O(U) \rangle = \frac{1}{Z} \int \mathcal{D}U \; O(U) \; \exp(-S(U)). \tag{2.2.14}$$

where here

$$\int \mathcal{D}U = \prod_x \prod_{\mu=1}^{4} \int \mathrm{d}U_\mu(x) \tag{2.2.15}$$

As the SU(N) matrices are unitary, we must use for $\mathrm{d}U_\mu(x)$ the invariant group measure or "Haar measure". It is gauge invariant and defined in depth in [3].

It is worth noting that in 2.2.14 the integrals over the link variables are over a compact domain and so this is well defined and finite without the need for the usual gauge fixing procedure. However as the integral is gauge invariant it is still possible to fix a certain gauge without affecting any observables. Starting from an arbitrary configuration of link variables it is possible to gauge certain subsets of links to the identity so that they contribute trivially to the action. Any set of links not containing a closed path can be gauged to 1. A gauge is fixed using what is known as a maximal tree which is a set of link variables that passes through every point on the lattice without any closed loops [4].

It is often found however, that fixing a gauge can increase the convergence time in a Monte Carlo simulation as it introduces long range interactions that are not well simulated [5]. Hence we will not fix a gauge for this analysis. We can renormalize the theory by fixing the value of a physical observable, such as the aforementioned string tension, to a physical value while varying the gauge coupling β as a function of a as $a \to 0$.

Chapter 3

Wilson Loops and Polyakov lines

In this chapter we will introduce the main observables we are interested in measuring, the Wilson Loop and the Polyakov loop and see how they can be used to analyse the confining behavior of an SU(2) gauge theory. For a more in dept discussion of the topics introduced here see [6] or [7].

3.1 Wilson Loops

We have established that the trace of the link variables around a closed loop is a gauge invariant quantity. The expectation value of such a loop is known as a Wilson Loop. For a path C, it is given by

$$W(C) = \langle \mathrm{tr} \prod_{(x,\mu)\in C} U_\mu(x) \rangle \tag{3.1.1}$$

where the product is over the links in the order are encountered along the path. We can think of the Wilson loop as measuring the response of the gauge group to a colour source travelling around its perimeter. For a timelike loop this represents a quark pair being created, travelling along the world lines of the loop and being annihilated at a later time.

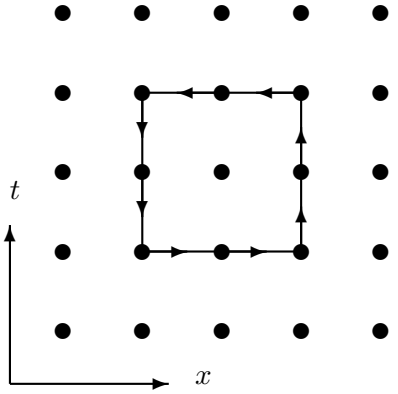

FIGURE 3.1: A 2 x 2 Wilson loop.

One defines the static quark potential $V(R)$ between two sources a distance R apart using a rectangular loop of size R x T. For this path, with two sides in the time direction of length T and two in a spatial direction of length R, we have

$$V(R) \equiv -\lim_{T\to\infty} \frac{1}{T} \log W(R,T) \tag{3.1.2}$$

For a detailed derivation of this result see [8]. It is worth noting that these Wilson loops are orientated, however reversing the orientation just corresponds to interchanging the quark and anti-quark.

On the lattice R and T are given by $R = na$ and $T = n_T a$ where $n(n_T)$ is the number of points in the spatial(time) direction. For large R and for strong coupling g, i.e. small β, we find that the potential increases linearly with R

$$V(R) \sim \sigma R. \tag{3.1.3}$$

In the large R, T limit the expectation value of the Wilson loops obeys an area law

$$W(R,T) \sim C\exp(-\sigma RT). \tag{3.1.4}$$

Here σ is the string tension. For large R we see a constant force acting between the two widely separated sources which is a clear indicator for static quark confinement. Physically, as the sources become widely separated, a flux tube with fixed radius and

energy density forms between them. This is due to the fact that the gluons interact with each other as opposed to QED for instance, where the flux lines spread out and the energy decreases with distance. With the introduction of dynamical quarks the analysis becomes more complicated as widely separated sources can reduce their energy by creating a new pair of quarks from the vacuum forming new colour singlets.

σ is a useful order parameter to distinguish between phases as it is always non-zero for confined phases, when the loops follow the area law, and is found to be zero for deconfined phases due to the sources no longer experiencing the long range potential.

In the weak coupling limit we find the potential has a $1/R$ form and so the total potential is given as

$$V(R) = A + \frac{B}{R} + \sigma R. \tag{3.1.5}$$

Numerically one can compute the string tension σ by first measuring the potential $V(R)$ versus R and extracting the string tension from the large R asymptotics. However at this stage the value of the lattice spacing is often not known so one actually plots $aV(an)$ versus n and extracts the dimensionless quantity $a\sqrt{\sigma}$. This is done by fitting the data to

$$aV(an) = Aa + \frac{B}{n} + \sigma a^2 n. \tag{3.1.6}$$

To find the value of the lattice spacing we introduce the Sommer parameter. The Sommer parameter r_0 is related to the force $F(R)$ between the two static quarks and is defined as

$$F(r_0)r_0^2 = 1.65 \tag{3.1.7}$$

Taking the derivative of $V(R)$ we find that, in lattice units

$$\frac{r_0}{a} = \sqrt{\frac{1.65 + B}{\sigma a^2}} \tag{3.1.8}$$

from which we can find a, using the physical value of $r_0 = 0.5$fm. It is found that the lattice spacing a decreases with increasing gauge coupling β.

Another possible way to compute the string tension, is shown in [9], where Creutz introduces a quantity $\chi(I, J)$ defined as

$$\chi(I, J) \equiv -\ln\left(\frac{W(I, J)(W(I-1, J-1)}{W(I, J-1)W(I-1, J)}\right). \tag{3.1.9}$$

which approximates the string tension for smaller loops of size I x J by eliminating any unwanted perimeter effects from the loops.

3.2 Polyakov Loops

Up until now we have taken all the dimensions of our Wilson loops to be much smaller then the dimensions of the lattice, to avoid unwanted effects due to the finiteness of the lattice. We include a non zero temperature in our analysis by decreasing the extent of the lattice in the time direction with respect to the spatial directions and by taking the temporal extent of our loops to be equal to that of the lattice. This results in a finite time integration in our Euclidean action and allows us to study our system at finite temperature $T = \beta_T^{-1}$.

$$S_E = \int \mathrm{d}^4x \; \mathcal{L} \longrightarrow \int_0^{\beta_T} \mathrm{d}t \int \mathrm{d}^3x \; \mathcal{L} \tag{3.2.1}$$

The temperature is related to the size of the lattice in the time direction as $T = \frac{1}{aN_t}$. This allows us to vary the temperature in two ways, by decreasing N_t or by decreasing the lattice spacing a. The latter can be done by increasing the inverse gauge coupling β which is a function of a as stated in the previous section. The previous case at zero temperature is recovered in the limit $\beta_T \to \infty$

With periodic boundary conditions in the time direction, an R x T Wilson loop with T equal to aN_t will wrap around the time dimension so that the two spatial lines will be on top of each other. These can be gauged to $\mathbb{1}$ and so we are left with two temporal loops, with opposite orientations.

A Polyakov loop is defined as the ordered product of the link variables along one such loop in the time direction, closed by the periodicity of the lattice

$$P(x) = \mathrm{tr}(\sum_{j=0}^{N_t-1} U_4(x)). \tag{3.2.2}$$

Due to spatial invariance, P, the spatial average of $P(x)$ is usually used in calculations. The expectation value of a Polyakov loop is related to the free energy F_q of our infinitely heavy test quark as

$$\langle P(x) \rangle \sim \exp(-F_q/T). \tag{3.2.3}$$

The correlator of two Polyakov loops allows us to study the static potential between two separated sources at temperature T and analyse the effect temperature has on its form,

$$\langle P(x)P(y)^\dagger \rangle = \exp(-V(R)/T), \tag{3.2.4}$$

where $R = x - y$. As the distance R between the sources goes to infinity we see

$$\langle P(x)P(y)^\dagger \rangle \longrightarrow |\langle P(x) \rangle|^2$$

and so for potentials of the form 3.1.3 $|\langle P \rangle|$ must vanish. This makes P another good order parameter. It is zero in confined phases when σ is non-zero and found to be non-zero in deconfined phases. By measuring $\langle P \rangle$ for increasing temperature one finds that pure SU(N) gauge theory undergoes a phase transition from a confined phase to a deconfined phase at critical temperature T_c. In the SU(2) case studied here, this phase transition is of second order, [10, 11].

Physically we can think of the Polyakov loops as measuring the screening of the source due to the surrounding gluonic medium. In the confined phase there can be no screening and so F_q is infinite, leading to zero $\langle P \rangle$ whereas in the deconfined phase F_q is finite due to screening, giving $\langle P \rangle \neq 0$.

Below the transition, in the confined phase we have a constant force between the sources for large R as before, however above T_c no such large R phenomena is found, signalling deconfinement.

$$V(R) \sim \begin{array}{ll} \frac{\alpha}{R} + \sigma R & \text{for } T < T_c \\ \frac{\alpha}{R}\exp(-\mu R) & \text{for } T > T_c \end{array} \tag{3.2.5}$$

With the introduction of dynamical fermions, $\langle P \rangle$ is no longer zero in the confined phase due to extra screening from the fermions and so the Polyakov loop is no longer a good order parameter.

3.3 Centre Symmetry

The Polyakov loops can also be used to show the spontaneous breaking of Z_n centre symmetry at the phase transition. We see from 3.2.2 that the Polyakov loop is a guage invariant quantity and so cannot be gauged away. However it is not invariant under what is known as a centre transformation. The centre of a group is the set of group elements that commute with all elements of the group. For SU(N) this is Z_n.

For a centre transformation we multiply all temporal link variables in a given time slice by an element z of the centre. Our action is invariant because it contains only traces of closed loops. Any z will come with a $z^\dagger$ and, because they commute with all elements of the group, they will cancel. So gauge configurations related by such a transformation will have the same statistical weight. The Polyakov loops does not transform so trivially. We find due to the fact that it winds around the compact time direction that it in fact transforms as

$$P \longrightarrow zP$$

Because of this we can write, in our SU(2) case, for non broken Z_2 symmetry

$$\langle P \rangle = \frac{1}{2}(P + zP) = \frac{1}{2}(1 - 1)P = 0 \tag{3.3.1}$$

and we see we have confinement. In the deconfined phase with $\langle P \rangle \neq 0$ we see that the centre symmetry is spontaneously broken and the Polyakov loop values should cluster around two distinct vacua.

3.4 Magnetic Monopoles and Centre Vortices

We have explained that confinement exists for widely separated quarks due to the linearly rising form of the potential they feel for large separations. We have suggested that this can arise if the colour field lines get collimated into a flux tube with constant cross-section between the quarks as the separation increases, as shown in Figure: 3.2. We would like to explain why the field lines take on this configuration. In this section I will briefly mention two classes of special field configurations which allow for this to happen, Centre Vortices and Magnetic Monopoles.

We know from the theory of superconductivity that the application of a magnetic field causes screening currents to form which expel the magnetic field from the interior of the superconductor. This is known as the Meissner effect and is due to the rearrangement of the cooper pairs in the superconductor. Above a critical value for the strength of the magnetic field B_c the currents can no longer expel the field and the superconductivity breaks down.

In a type II superconductor this transition from a superconducting to a non superconducting state doesn't happen at a single value of the magnetic field as it does in a type I superconductor. There is an intermediate phase, between two critical values of the magnetic field B_{c_1} and B_{c_2} where certain regions in the superconductor are still superconducting. In this phase the magnetic field can penetrate and form flux tubes inside the superconductor. A pair of a magnetic monopole and an anti-magnetic monopole in the superconductor, provided they existed, would then form a configuration like the

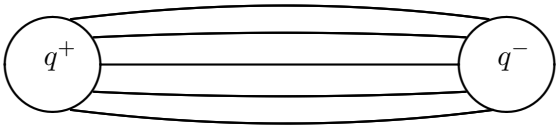

FIGURE 3.2: The flux tube between a separated quark and anti-quark pair.

quark antiquark pair in Figure: 3.2. They would feel a linear potential and would be confined in the same sense as the quarks.

In analogy, 't Hooft and Mandelstam suggested that the QCD vacuum could be thought of as a dual superconductor, ie. one where electric and magnetic phenomena have been reversed. The lines of "electric" colour flux between a quark and antiquark are confined to the flux tube due to circulating "magnetic" colour charges in the vacuum as opposed to the magnetic flux being confined to the flux tubes between magnetic charges due to circulating electric currents in a standard superconductor.

This then begs the question of whether we can explain the existence of these vacuum magnetic colour charges in confining phases of our theory. In some lattice simulations of $U(1)$ gauge theories monopoles are indeed found to be abundant in confined phases and scarce in deconfined phases. For non abelian theories their appearance can be explained in the "maximal abelian gauge" as $U(1)$ Dirac monopoles, [12].

We have explained in section 3.3 how the deconfinement transition at T_c can be related to the spontaneous breaking of centre symmetry. A second possible mechanism for confinement, suggested by 't Hooft(1979), Mack(1979) and Ambjorn(1980), is related to the condensation of "centre vortices" or magnetic flux tubes in the confined phase.

In [13] 't Hooft introduced an operator $B(C)$ that creates a centre vortex. $B(C)$ can be thought of as a loop dual to the Wilson loop, called the 't Hooft loop. The two loops are related via an element z of the centre as

$$B(C)W(C') = zW(C')B(C). \tag{3.4.1}$$

It is in a deconfined phase that a 't Hooft loop obeys the area law 3.1.4 and in the confined phase it obeys a perimeter law [14]. In the centre symmetric phase abundant centre vortices percolate through the vacuum and ensure the Wilson loops follow the area law leading to the correct confining behavior of the colour sources.

Chapter 4

Monte Carlo Simulations

4.1 Importance Sampling and the Monte Carlo Method

Our goal is to measure expectation values of observables, such as the Wilson or Polyakov loops, which are functions of the gauge field on the lattice.

The number of link variables for any reasonably sized lattice will be very large. As an example, a lattice with 10^4 points will have 40000 link variables. Even for the simplest gauge theories this leads to an enormous amount of different possible configurations. For example a Z_2 gauge theory would have 2^{40000}. Computing observables with 2.1.14 would then involve a partition function sum over all these configurations and this is just too much to deal with computationally.

What is needed is a way to reduce this sum to something more manageable. We note that each term in the partition function is weighted with a Boltzmann weight, which depends on the value of the action for that particular configuration. In this way some terms will have larger weights than others and are more 'important' in the sense that they will contribute more to the sum.

Importance sampling of the configurations allows us to approximate the huge sum by a smaller subset of N configurations U with large Boltzmann weight. Expectation values can then be computed using the average of the observable evaluated on these N sample configurations of the field.

$$\langle O \rangle \approx \frac{1}{N} \sum_{U} O(U) \tag{4.1.1}$$

4.2 Markov Chains

We want to generate an ensemble of configurations according to a probability distribution density proportional to the Boltzmann factor

$$dP(U) \sim \exp(-\beta S(U)) dU \tag{4.2.1}$$

This is done by generating a sequence of configurations from an initial configuration U_1.

$$U_1 \to U_2 \to U_3 \to ...U_N$$

When a new configuration is generated it is known as an update or step. At any point in the process the next configuration to be generated depends only on the previous one and as the process goes on the configurations tend towards those with bigger Boltzmann weight. This is a stochastic process and the probability $T(U'|U)$ to transition from a configuration U to U' must obey

$$1 \geq T(U'|U) \geq 0 \qquad \sum_{U'} T(U'|U) = 1 \tag{4.2.2}$$

We want to ensure that, after a while, as the sequence approaches an equilibrium distribution $P(U)$ there are no sinks or sources of probability. We insist that the probability to go from U to U' when the system is in the configuration U is equal to that of going from U' to U when the system is in the configuration U'.

$$\sum_{U} T(U'|U) P(U) = \sum_{U} T(U'|U) P(U'), \tag{4.2.3}$$

We must also insist that there is a non-zero probability to transition from U to U' for all U'. This is known as strong ergodicity and tells us that all possible configurations can be reached in a finite number of updates.

$$T(U'|U) \geq O \; \forall \; U' \tag{4.2.4}$$

A process satisfying 4.2.2, 4.2.3 and 4.2.4 is known as a Markov process and the sequence of configurations is known as a Markov chain.

4.3 The Metropolis Algorithm

There are a number of different algorithms used to generate Markov chains, the simplest, due to Metropolis et al. [15], being the Metropolis Algorithm. It involves three basic steps:

1. Starting with configuration U_N, generate a trial configuration U_{N+1} according to the selection probability $T(U_{N+1}|U_N)$
2. The new configuration is then accepted with the acceptance probability

$$T_A(U_{N+1}|U_N) = \min\left(1, \; \frac{T(U_N|U_{N+1})\exp(-S(U_{N+1}))}{T(U_{N+1}|U_N)\exp(-S(U_N))}\right) \tag{4.3.1}$$

3. Repeat the previous two steps using the new value if it has been accepted or the original value if not.

The original configuration can be chosen in a number of ways. One possible choice is to set all link variables to the identity which is known as a cold start. Another possibility, a hot start, is where the links are all chosen randomly.

In our SU(2) case with Wilson's action subsequent candidate configurations are generated by multiplying the value of one of the link variables by X, a randomly chosen member of the gauge group. It is usually taken to be close to the identity so that the acceptance probability does not get too small.

$$U_\mu(x) \longrightarrow XU_\mu(x) = U_\mu(x)' \tag{4.3.2}$$

In four dimensions each link is shared by six plaquettes. The change in the action due to updating one link is computed using

$$\Delta S = -\frac{\beta}{N}\text{Re tr}[(U_\mu(x)' - U_\mu(x))A] \tag{4.3.3}$$

Here A is the sum over the staples which are the products of the other link variables in the plaquettes containing $U_\mu(x)$, shown in Figure: 4.1.

$$A = \sum_{\mu\neq\nu} U_\nu(x+\hat{\mu})U_\mu^\dagger(x+\hat{\nu})U_\nu^\dagger(x) + U_\nu^\dagger(x+\hat{\mu}-\hat{\nu})U_\mu^\dagger(x-\hat{\nu})U_\nu(x-\hat{\nu}). \tag{4.3.4}$$

A random number r between 0 and 1 is then generated. The new value $U_\mu(x)'$ is accepted if $r \leq \exp(-\Delta S)$ or discarded otherwise. This ensures that the new value is always chosen if the action decreases or remains the same but also allows configurations with an increased action to be accepted occasionally. The process then repeats for another link on the lattice. Updating each link on the lattice is known as a sweep over the lattice.

After a number of updates the system thermalises and the configurations obey 4.2.1. Once the system is in equilibrium an ensemble of configurations can be generated to use in 4.1.1.

In principal the Metropolis algorithm can be used to study any system, however there can be better methods depending on what is to be simulated. This is because the Metropolis algorithm is what is known as a local Monte Carlo algorithm. Each update only affects a few variables locally. This can lead to long running times for the whole phase space of configurations to be sampled and many updates must be performed

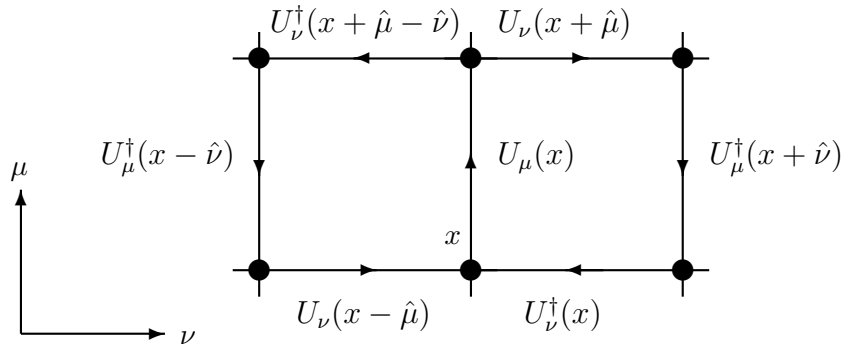

FIGURE 4.1: The two plaquettes in the μ - ν plane which contain $U_\mu(x)$.

in between measurements to ensure they are not correlated. Methods to deal with correlated measurements will be discussed in section 4.5.

4.4 The Heat Bath Algorithm

An improved method, known as the Heat Bath algorithm, optimises the acceptance rate of the new configurations. It is known as such because it simulates touching the link variables with a heat bath, which will eventually bring our system into equilibrium at inverse temperature β_T. The main idea is to combine the first two steps in the Metropolis algorithm into one. We note again that when updating a link only the six plaquettes containing the link will change. We find that 4.2.1 becomes

$$\mathrm{d}P(U) \sim \mathrm{d}U \, \exp\left[\frac{1}{2}\beta \mathrm{Tr}\left(U \sum_{\alpha=1}^{6} \tilde{U}_\alpha\right)\right] \tag{4.4.1}$$

where $\tilde{U}_\alpha$ are the six staples containing U. This algorithm lends itself well to the study of SU(2) gauge theories due to the fact that for SU(2) the sum of two group elements is proportional to another, so we have,

$$\sum_{\alpha=1}^{6} \tilde{U}_k = k\overline{U}, \quad \text{where} \quad k = \left|\sum_{\alpha=1}^{6} \tilde{U}_\alpha\right|^{1/2} \tag{4.4.2}$$

The heat bath algorithm is then:

1. Compute $\overline{U}$ from the staples containing the link to be updated.
2. Generate a group element according to the distribution 4.4.1.
3. Take the new value for the link as $U' = U\overline{U}^{-1}$ and repeat for the next link.

Using the standard pauli matrices σ, we parameterize the elements as

$$U = a_0 I + i\vec{a} \cdot \vec{\sigma}, \qquad a_0^2 + \vec{a}^2 = 1. \tag{4.4.3}$$

We need then only generate points on the four dimensional unit sphere, with appropriate weighting in the a_0 direction, to use in step 2.

The heat bath algorithm is useful in that it reaches equilibrium quicker than any other Monte Carlo algorithm that only changes one link at a time, however all other valid algorithms will eventually simulate the heat bath after enough iterations. To decrease computing time and correlations between subsequent measurements further the heat bath algorithm can be coupled with other methods such as checker boarding, where more than one link is updated at once. Other methods such as the Langevin Algorithm or the Molecular Dynamics method also exist, as detailed in [6].

4.5 Error analysis and autocorrelation

For a set of N random data $X_1, ..., X_N$ one computes the mean and variance using

$$\hat{X} = \frac{1}{N}\sum_{i=1}^{N} X_i, \quad \hat{\sigma}^2 = \frac{1}{N-1}\sum_{i=1}^{N}(X_i - \hat{X})^2. \tag{4.5.1}$$

For uncorrelated data these are good estimators for the actual value of the expectation value and variance of our observable. We then get as the final value of our observable, with statistical error σ,

$$X = \hat{X} \pm \sigma, \quad \sigma = \frac{\hat{\sigma}}{\sqrt{N}}. \tag{4.5.2}$$

This is only accurate for N independent measurements. However in measuring observables on lattice configurations generated in a Markov process one often finds that subsequent measurements are in fact not uncorrelated. We note that the error decreases as the square root of the number of independent measurements.

To measure the extent of this correlation between subsequent measurements one defines the autocorrelation coefficient between two measurements, k measurements apart, as

$$C_k = \frac{1}{N}\sum_{i=1}^{N-k}(X_i - \hat{X})(X_{i+k} - \hat{X}_{i+k}) \tag{4.5.3}$$

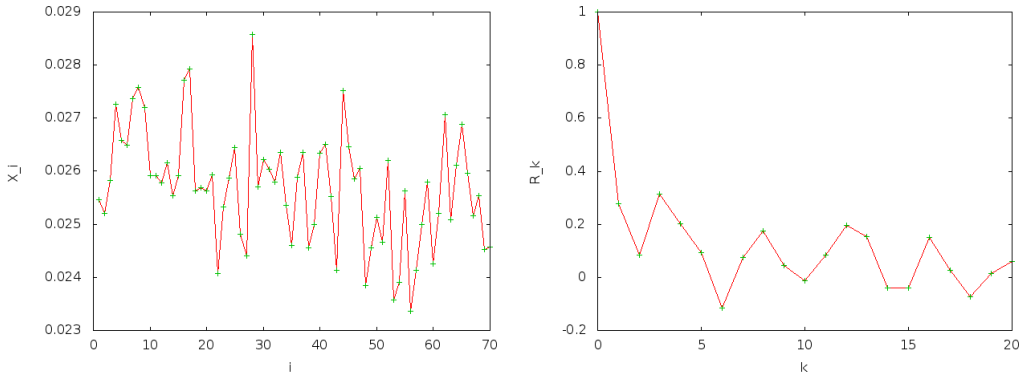

FIGURE 4.2: A data set and its correlogram. We see here that after four updates the measurements are uncorrelated enough to be considered statistically independant.

One then computes the normalized coefficient $R_k = C_k/C_0$. A plot of R_k versus k known as a correlogram shows exponentially decaying behavior and can be used to estimate the autocorrelation time t using

$$R_k \sim \exp(-k/t). \tag{4.5.4}$$

Measurements separated by more than t can be then taken to be independent and 4.5.2 can be used, [16].

4.6 Summary

To summarize on what has been said so far:

1. We start with the action for the theory we want to study numerically and translate it to Euclidean time via a Wick rotation.

2. We then discretize this action on a spacetime lattice such that in the limit of the lattice spacing going to zero, we arrive back at our original continuum theory.

3. With our discretized Euclidean action we define a partition function as a sum over configurations of our field on the lattice.

4. An ensemble of configurations of the field, exponentially weighted by the action, are generated using an appropriate Monte Carlo algorithm.

5. Finally, any observables wanted are computed as averages over the values from this ensemble of field configurations.

Chapter 5

Results

In this chapter I will present results from numerical simulations with Wilson's action. The code used was based on one written by Michael Creutz which is available to download at *latticeguy.net*. All errors were computed as shown in chapter 4.

5.1 String tension at zero temperature

To determine the value of the string tension at zero temperature square Wilson loops of side n for $n = 1, ..., 5$ were measured on a 16^4 lattice. We note that technically on a finite lattice the temperature is not actually zero however keeping the dimension of the lattices large compared to the Wilson loop approximates the zero temperature case.

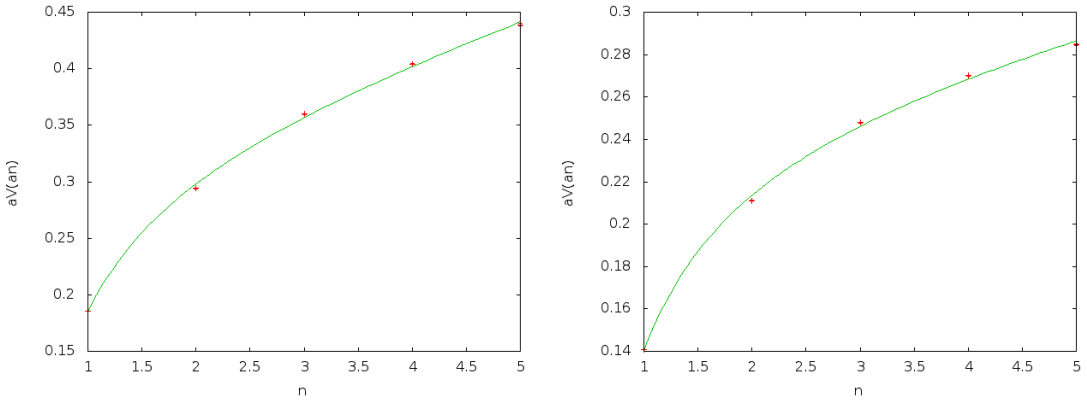

FIGURE 5.1: Numerical data for the static quark potential for $\beta = 2.5$ and $\beta = 3$

The potential in lattice units $aV(na)$ where $R = na$ versus n is shown in Figure 5.1. The data was taken from 300 measurements performed every 5 sweeps over the lattice.

We can see the expected linear form of the potential associated with confinement for larger n. For small n we can also see evidence of the short distance Coulomb form of the potential. The data was fitted to 3.1.6 and used to compute the string tension in lattice units, $a\sqrt{\sigma}$ and lattice spacing a as shown in section 3.1.

We find from the fit, for $a\sqrt{\sigma}$, a value of 0.177 ± 0.009 for $\beta = 2.5$. This value is consistent with those found in the literature [17]. This value of the string tension corresponds to a lattice spacing of 0.072738 ± 0.000002 fm. In the second case, for $\beta = 3$, values for $a\sqrt{\sigma}$ and the lattice spacing a are found to be 0.110 ± 0.009 and 0.04434 ± 0.000002 fm respectively. Here we can clearly see that the lattice spacing decreases with increasing β.

5.2 Phase transition at non-zero temperature

To simulate the SU(2) gauge field at non-zero temperature the measurements were performed on a 4 x 16^3 lattice. In Figure 5.2 the expectation value of the Polyakov loop, $\langle|P|\rangle$, is shown versus the gauge coupling β around the phase transition.

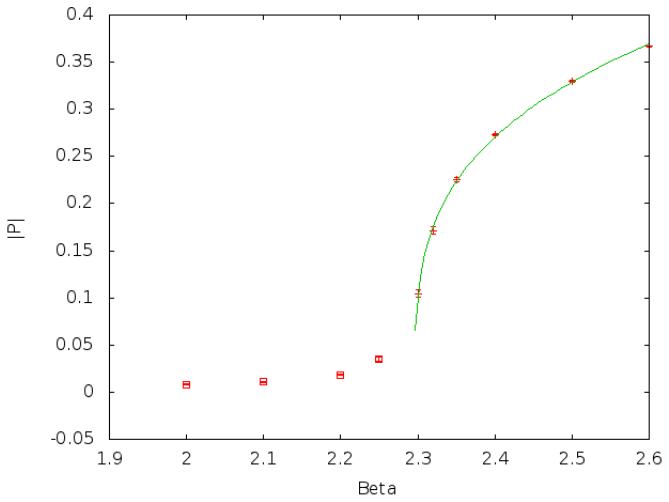

FIGURE 5.2: Expectation value of the Polyakov loop as a function of the inverse gauge coupling β.

As we have shown in the previous section, an increase in β corresponds to a decrease in the lattice spacing. From our relation for the temperature $T = (aN_t)^{-1}$ we see the increase in β corresponds to an increase in temperature. At approximately $\beta = 2.3$ we see evidence that the system undergoes a phase transition from a confined to a deconfined phase. The expectation values for the Polyakov loops are no longer zero signalling deconfinement as explained in section 3.2. Fitting the data above the transition to a curve of the form

$$f(\beta) = C(\beta - \beta_c)^a \tag{5.2.1}$$

we find a value for β_c of 2.2962 ± 0.0005. This agrees quite closely with the value of 2.2986 ± 0.0006 found in the literature [17].

This phase transition can also be seen from the distribution of the actual measured values of the Polyakov loops on the lattice. Below the phase transition, at $\beta = 2.25$ shown in Figure 5.3, we see that the values are equally distributed about zero as expected. Here

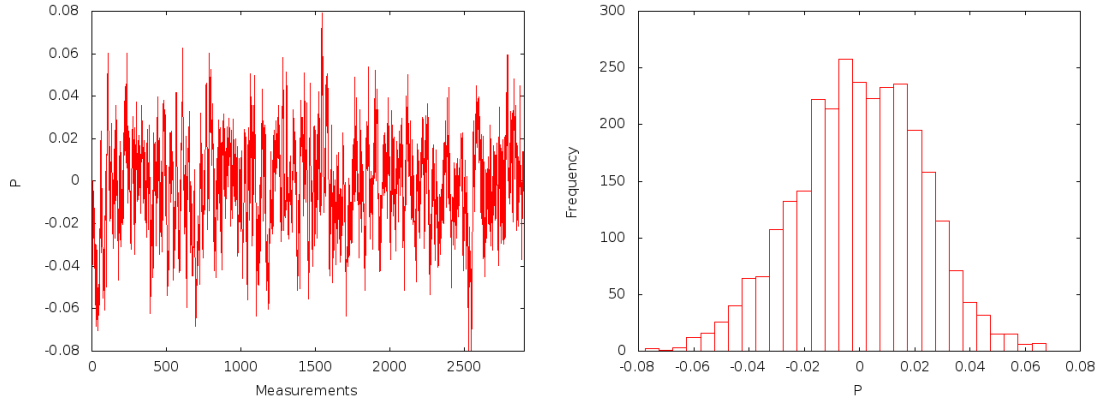

FIGURE 5.3: Measured values of P on the lattice and the frequency each occurs for $\beta = 2.25$.

we can see that the Z_2 centre symmetry is unbroken, and the expectation value of the Polyakov loop is zero, which is expected in the confined phase, as explained in Section 3.3.

In Figure 5.4, just above the phase transition at $\beta = 2.3$, we see that the values measured are distributed about two values or "centre phases" due to the spontaneous breaking of the Z_2 centre symmetry. Looking at the first plot in Figure: 5.4 we see that the system spends a period of time "stuck" in one phase before tunneling to the other. We expect for an infinite run that the system would spend an equal amount of time in both phases leading to a zero expectation value, hence the need to use $\langle |P| \rangle$ as opposed to $\langle P \rangle$ to determine the value of β at the phase transition. Far above the phase transition the tunneling is less of an issue. At $\beta = 2.35$ as shown in Figure: 5.5 we can see that the

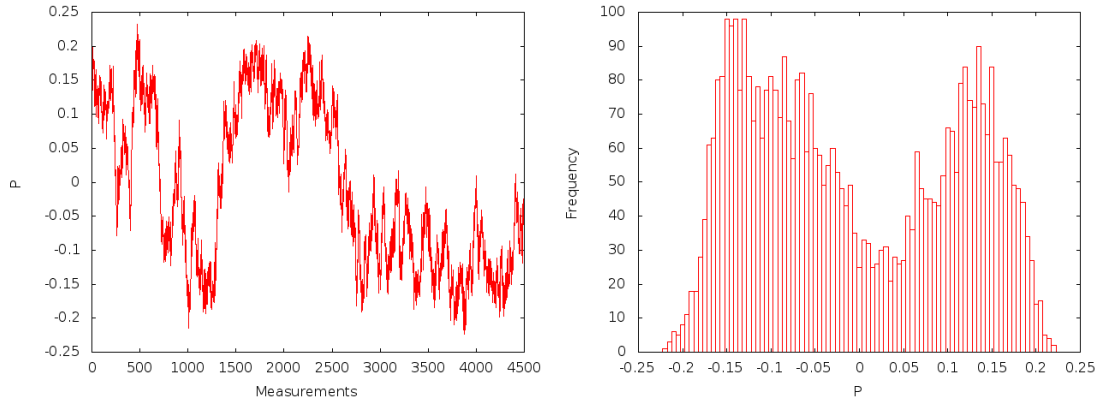

FIGURE 5.4: Measured values of P on the lattice and the frequency each occurs for $\beta = 2.3$

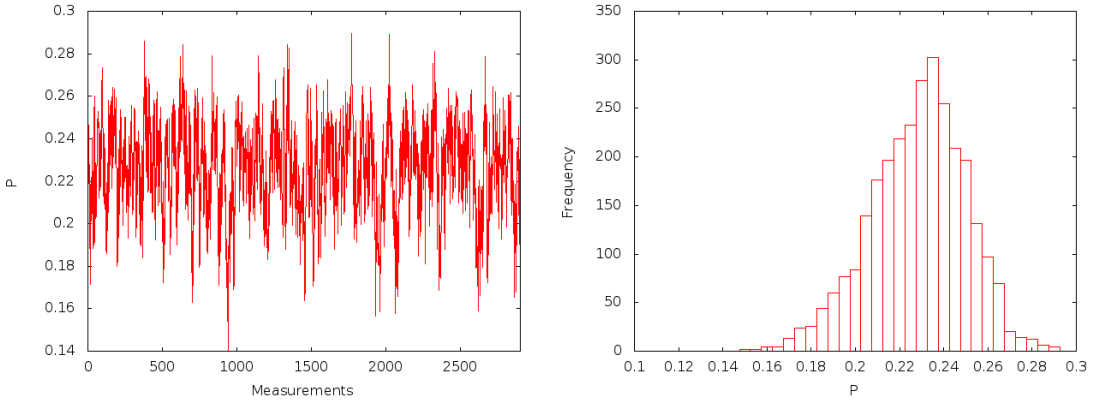

FIGURE 5.5: Measured values of P on the lattice and the frequency each occurs for $\beta = 2.35$

system has settled down into one of the two centre phases and stays there long enough to provide an accurate estimation for the value of P.

The data here have been taken on runs of between 1000 and 5000 measurements, each separated by five sweeps over the lattice. Close to the phase transition the system takes longer to thermalise and subsequent measurements are much more strongly correlated so larger data sets are needed to perform adequate statistics.

We see from Figure 5.6 that far from the transition, at $\beta = 2$ each gauge configuration is uncorrelated and so each measurement can be taken as independent. At $\beta = 2.25$, much closer to the transition, we find from fitting the data via 4.5.4 a value of 28 for t. That is, after 28 measurements the data are uncorrelated enough to be considered independent.

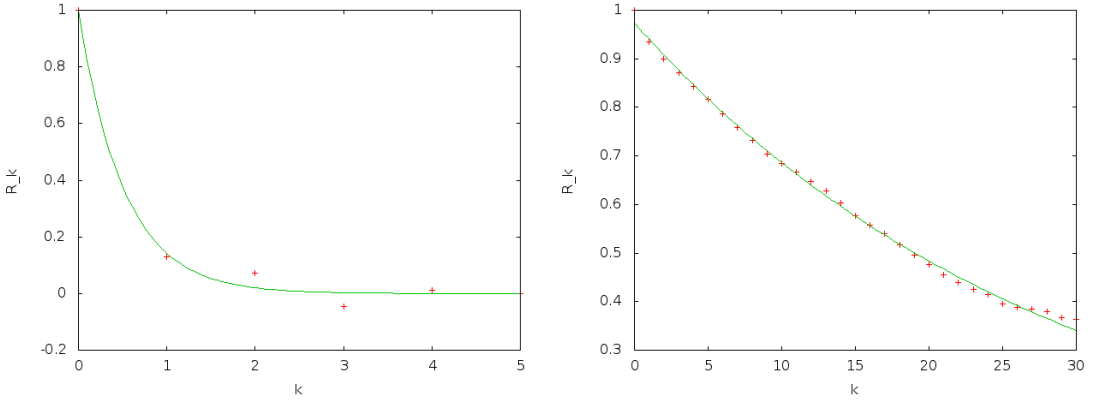

FIGURE 5.6: Correlogram for $\beta = 2$ and $\beta = 2.25$

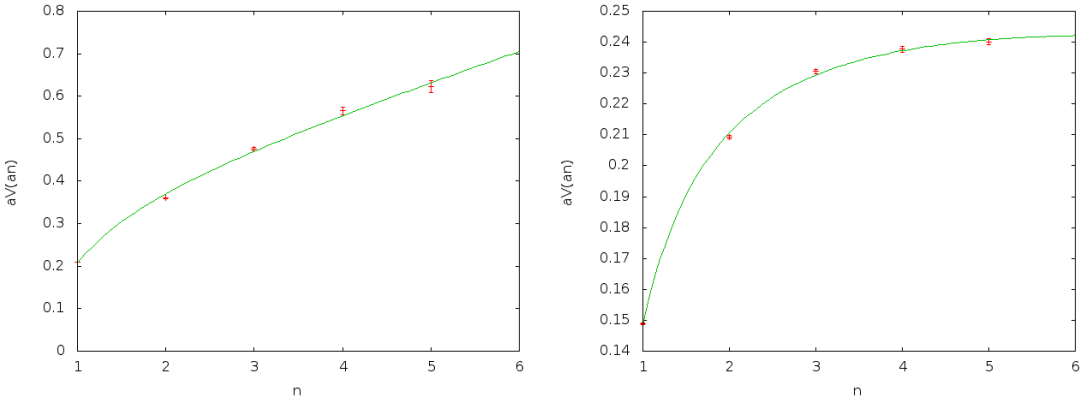

FIGURE 5.7: Numerical data for the static quark potential for $\beta = 2.25$ and $\beta = 2.5$

In Figure: 5.7 we see the static quark potential for values of β above and below β_c. The potential was computed from rectangular Wilson loops of size n_t x n for $n_t = 4$ and $n = 1, ..., 5$. For $\beta = 2.25$ we can clearly see the potential is rising linearly for larger R. The value for the string tension is found to be $a\sqrt{\sigma} = 0.26 \pm 0.02$. In the second case for $\beta = 2.5$ for larger R we see the potential levels off, signalling a zero string tension and deconfinement.

In Figure: 5.8 we see a rough plot of $a^2\sigma$ versus β about the transition. In it we can clearly see that the string tension goes to zero above the deconfining temperature, as expected in the deconfined phase.

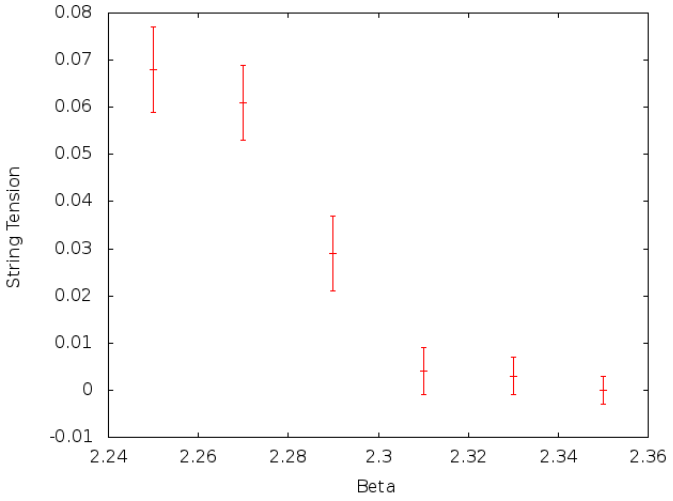

FIGURE 5.8: Numerical data for $a^2\sigma$ versus the inverse coupling β

Chapter 6

Discussion and Further Analysis.

In the course of this dissertation we have seen how a gauge theory can be discretized on a lattice and how this non-perturbative regularization scheme can be used as a way to study aspects of a theory unavailable to standard perturbative investigations, even on the most basic of personal computers today. Divergent integrals were replaced with finite sums and the expectation values of observables were found as averages over the values computed on an ensemble of field configurations generated in Monte Carlo simulations.

We have measured Wilson Loops of various sizes for pure SU(2) gauge theory at zero and non-zero temperature and used them to compute the potential felt between a pair of separated colour sources. This potential was found to rise linearly for larger separations below a critical temperature, consistent with the assumption that quarks are confined at low energies. The string tension σ found from this potential was measured and shown to be a good order parameter, useful in distinguishing between confined and deconfined phases.

A second order parameter, the Polyakoy loop, was also measured for a range of values of the coupling constant. From this we have seen that on a lattice with $n_t = 4$ the theory undergoes a phase transition from a confined to a deconfined phase at the critical inverse coupling $\beta_c = 2.2962 \pm 0.0005$. We have also seen how this phase transition can be related to the spontaneous breaking of centre symmetry. In the confined phase we found that the expectation value of the Polyakov loop is indeed zero, consistent with the idea that the centre symmetry is not broken. Above the phase transition the

symmetry is found to be spontaneously broken and the Polyakov loop takes on a non zero expectation value.

There are a number of opportunities for further study of the material discussed here. Larger lattice sizes and running times would allow for a more accurate determination of the string tension, by reducing the statistical error related to the number of uncorrelated measurements. Longer running times when computing the expectation value of the Polyakov loop would lead to less errors due to the tunneling between centre phases. Repeating the calculation of the critical coupling for different values of n_t would allow us to compare how the lattice size affects the transition. Finally an investigation of the effects twisted boundary conditions on the lattice would have on the string tension could be considered.

Acknowledgments

I would like to thank Dr. Rajantie for agreeing to supervise this dissertation and for his many helpful insights along the way. I would also like to thank Dr. David Weir for answering many questions related to the coding aspects of this dissertation.

Bibliography

[1] K. G. Wilson. Confinement of quarks. *Phys. Rev. D 10*, 1974.

[2] M. Peskin and D. Schroeder. *An Introduction to Quantum Field Theory*. Westview Press, 1995.

[3] J. Smit. *Introduction to Quantum Fields on a Lattice*. Cambridge University Press, 2002.

[4] M. Creutz. *Quarks, Gluons and Lattices*. Cambridge University Press, 1983.

[5] M. Creutz. Monte Carlo study of quantized SU(2) gauge theory. *Phys. Rev. D 21*, 1980.

[6] H. J. Rothe. *Lattice Gauge Theories: An Introduction*, volume 82 of *World Scientific Lecture Notes in Physics*. World Scientific, 2012.

[7] J. I. Kapusta and C. Gale. *Finite Temperature Field Theory Principles and Applications*. Cambridge Monographs on Mathematical Physics. Cambridge University Press, 1989.

[8] I. Montvay and G. Münster. *Quantum Fields on a Lattice*. Cambridge University Press, 1994.

[9] M. Creutz. Asymptotic-Freedom Scales. *Phys. Rev. Lett.*, 1980.

[10] J. Kuti, J. Polonyi and K. Szlachanyi. Monte Carlo study of SU(2) gauge theory at finite temperature. *Phys. Lett. 98B*, 1981.

[11] L. D. McLerran and B. Svetitsky. A Monte Carlo study of SU(2) Yang-Mills theory at finite temperature. *Phys. Lett. 98B*, 1981.

[12] G. 't Hooft. The Topological Mechanism for Permanent Quark Confinement in a Non-Abelian Gauge Theory. *Physica Scripta.*, 1982.

[13] G. 't Hooft. On the phase transition towards permanent quark confinement. *Nucl. Phys. B138*, 1978.

[14] P. de Forcrand. 't Hooft loop, electric flux sectors, and confinement in SU(2) Yang-Mills theory. *Phys. Rev. D 66*, 2002.

[15] Metropolis et al. Equation of State Calculations by Fast Computing Machines. *The Journal of Chemical Physics*, 1953.

[16] C. Chatfield. *The Analysis of Time Series, An Introduction.* Texts in Statistical Science. Chapman and Hall, 1975.

[17] M. J. Teper. Glueball masses and other physical properties of SU(N) gauge theories in D=3+1: a review of lattice results for theorists, 1998.